

Microstructure and Mechanical Properties of Cold Sprayed Amorphous Coating

Wojciech C. Żórawski^{1*}, Martin Vicen², Anna Trelka-Druzic³, Anna Góral³,
Medard Makrenek⁴, Stanisław Adamczak¹, Otakar Bokuvka²

¹ Faculty of Mechatronics and Mechanical Engineering, Kielce University of Technology, Tysiąclecia Państwa, Polskiego 7, 25-314 Kielce, Poland

² Department of Materials Engineering and Research Centre, Faculty of Mechanical Engineering, University of Zilina, 010 26 Zilina, Slovakia

³ Institute of Metallurgy and Materials Science, Polish Academy of Sciences, 30-059 Kraków, Poland

⁴ Faculty of Management and Computer Modelling, Kielce University of Technology, Tysiąclecia Państwa, Polskiego 7, 25-314 Kielce, Poland

* Corresponding author's e-mail: ktrwz@tu.kielce.pl

ABSTRACT

Metallic glasses, especially those based on zirconium have garnered significant attention due to their unique amorphous structure, offering a combination of high strength, corrosion resistance, and unique wear properties. The cold spray process, a solid-state coating deposition method, has emerged as a promising technique for applying metallic glass coatings, preserving the amorphous structure. The presented studies aimed to analyze the microstructure and mechanical properties of a cold sprayed Zr-based amorphous powder. The coating was sprayed using the Impact Innovations 5/8 system with the robot Fanuc M-20iA at Kielce University of Technology. The feedstock used for this study was commercial AMZ-4 powder. The high kinetic energy of feedstock particles and their morphology caused significant deformation, and particular splats strongly adhered to the substrate and each other. Throughout the cross-section, the coating was homogenous and exhibited negligible porosity. On the other hand, histograms and probability distributions of the hardness and Young's modulus of cold sprayed coating showed significant differences. X-ray diffraction analysis indicated that the deposited coating had the same amorphous structure as the feedstock.

Keywords: cold spraying, amorphous coating, microstructure, mechanical properties.

INTRODUCTION

The development of coatings with significantly better properties has always been associated with research on new materials and new surface engineering technologies, which has allowed for their more effective application. Metallic glasses, in comparison with traditional materials, possess a number of properties that make them very interesting for new applications in various industries. These unique properties include, among others; high wear and corrosion resistance, high hardness, and elastic modulus. These properties result

from the short-ordered structure, in contrast to the classical crystalline structure of commonly used metals and alloys. It is precisely the absence of grain boundaries, which cause reduced properties of crystalline materials, that is the reason for their significantly better wear and corrosion resistance [1–3]. Their production involves a rapid cooling process (> 10 K/s), preventing an ordered crystalline structure formation. Such a process can be carried out but only for very small volumes of material due to the possibility of very rapid heat dissipation so as not to allow its crystallization. Therefore, amorphous materials are often

produced in the form of powders, tapes or wires, significantly limiting their application possibilities. Another problem is the limited plasticity of metallic glasses, resulting from their special atomic structure. Therefore, no slip bands occur in the case of deformations as in crystalline materials. As a result, this leads to the formation of brittle cracks at a much lower stress level than in the case of traditional materials. Therefore, processes that would allow coatings deposition directly onto machine parts while preserving their amorphous structure and assumed dimensions are particularly interesting. This would eliminate the need for additional plastic deformation [4–6].

New possibilities in the deposition of amorphous coatings have been created by the breakthrough cold gas spraying process, developed in the 1980s. The cold spray process was originally developed in the mid-1980s at the Institute of Theoretical and Applied Mechanics of the Russian Academy of Science in Novosibirsk by Prof. Anatolij Papyrin and his colleagues [7, 8]. In this process, metal powder of relatively small particles (1–50 μm in diameter) is applied to deposit a coating. Powder particles are injected into a high-velocity gas stream (300–1200 m/s) and accelerated towards the substrate (Figure 1a). Upon impact, the particles in the solid state (opposite to other thermal spray processes where particles are plastic or molten after heating) deform to form a splat and create a bond with the substrate. Subsequent new particles impact the substrate and form bonds with previously sprayed and deformed particles. This process occurs after the powder particles exceed the critical velocity v_{cr} . The degree of

particle deformation is very high because of the very high speed of the powder particles, despite the lack of heating. As a result, a uniform coating with a small number of pores and very high adhesion and cohesion is formed. The cold gas spraying process and the coatings obtained have several advantages, including: phase composition stability, high density, low oxide content, low residual stresses, high deposition rate, minimal substrate heating, preservation of the nanocrystalline structure of sprayed nanomaterials, high hardness compared to traditional coatings [10–12]. Coatings can be deposited using low-pressure systems operating at pressure of 0.6–1.0 MPa and temperatures of up to 550 $^{\circ}\text{C}$ [13], as well as high-pressure systems at 5 MPa and 1100 $^{\circ}\text{C}$, respectively (Figure 1b). High-pressure systems (Fig. 1b) allow for the use of a wider range of powders, and the coatings have significantly better properties [14–17]. This process also allows for the use of amorphous powders. Metallic glasses can be produced in this process because the temperature of amorphous powders does not exceed the glass transition temperature, which allows for superplastic deformation ability and maintenance of the amorphous structure of the feedstock. Other thermal spray technologies (plasma, HVOF) do not ensure complete preservation of the amorphous structure because crystalline phases appear in the coatings [18, 19]. There are studies on the properties of cold sprayed iron-, aluminum-, nickel-, and copper-based amorphous coatings in the literature [20–23]. Some works are devoted to using amorphous Zr-based AMZ4 powder for laser additive manufacturing bulk metallic glasses

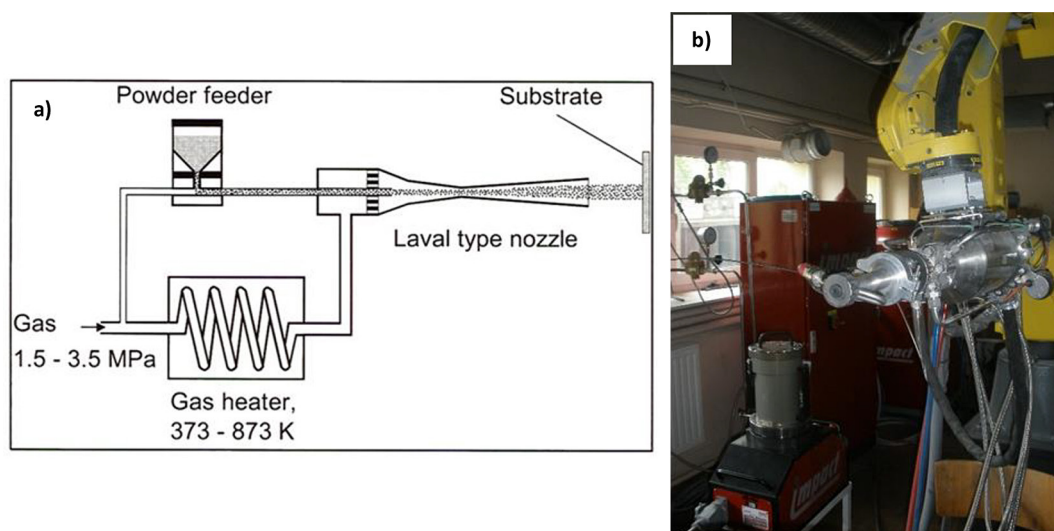


Figure 1. Cold spray: (a) schematic [9], (b) Impact Innovations 5/8 high-pressure system

[24–27]. However, there is very little research in on the properties of Zr-based cold sprayed coatings, especially dedicated to the possibilities of using amorphous AMZ4 powder in this process.

MATERIALS AND METHODS

Commercial amorphous powder AMZ4 ($Zr_{59.4}Cu_{28.8}Al_{10.4}Nb_{1.5}$, at.%) was applied as feedstock in this study (Heraeus AMLOY Technologies GmbH). Crystallization temperature of powder was 472.2 °C [28]. The particle size distribution of this powder was tested with a HELOS H2398 laser diffractometer from Sympatec GmbH. Cold spray process was performed with an Impact Innovations 5/8 System in cooperation with a Fanuc M-20iA robot. Gas mixture 50% nitrogen and 50% helium was used as the process gas to deposit amorphous coating. The maximum system parameters including temperature 800 °C and pressure 3.5 MPa were applied to ensure the maximum velocity and temperature of the amorphous powder grains. The coating was deposited with a stand of distance onto a 1H18N9T steel with dimensions of 400 × 30 × 5 mm. The nozzle traverse speed was 400 mm/s, and the deposition step size was 2 mm. To obtain the appropriate thickness of coating two layers were deposited on sample. The deposition process involved cooling the specimens and keeping them at a temperature of below 80 °C (Testo Quicktemp 850-2 laser thermometer). The substrate preparation before the cold spraying process includes degreasing and sandblasting with EB14 electro corundum under 0.5 MPa air pressure. For metallographic studies a sample of the deposited coating was cut using an “ISOMET – low-speed saw” (BUEHLER) equipped with a diamond blade. Next, the AMZ4 powder and coating samples were embedded in resin and then polished with increasingly fine, i.e. 3 μm, 1 μm and 0.25 μm, diamond suspensions on a “LaboPol – 5” (STRUERS) polishing machine. A SEM microscope Jeol JSM-7100F and Jeol JSM 5400 equipped with an ISIS 300 Oxford (EDS) microprobe for chemical composition analysis were used to analyse the microstructure of the powder and the deposited coating. The coating porosity was determined through image analysis according to ASTM-E2109. The phase composition of the powder and as-sprayed deposit was studied using a Bruker D8 Discover diffractometer, while that of the powder feedstock

using a Philips X’Pert PW 1710 diffractometer equipped with the Diffrac. EVA V3.0 and High-Score Plus 4.8 software with the ICDD PDF-4+ crystallographic database. Co-K α radiation ($\lambda = 1.78897 \text{ \AA}$) was used in both cases. The micromechanical tests have been carried out on polished cross-sections of the deposited coating by means of a Nanovea tester with a Berkovich indenter (the Olivier and Pharr methodology), 20 mN applied load and 50 mN/min loading rate. Forty nine measurements were made on each cross-section of the cold sprayed amorphous coating. The hardness (HV0.3) of the coating was measured using the Innovatest Nexus 4000 tester (Innovatest, Maastricht, Netherlands). Five readings were carried out for each coating. The morphology of the as-sprayed coating was analyzed using a Talysurf CCI-Lite non-contact 3D profiler.

AMZ4 amorphous powder

AMZ4 amorphous powder was used in the cold spray process to deposit the coating. From Figure 2a, it can be seen that the particles are spherically and irregularly shaped, which is characteristic of the high-pressure inert gas atomization process. Most of grains have a smooth surface, but the surface of larger grains has irregularities resulting from insufficient atomisation (Figure 2c). Very fine satellite particles are also visible, most of which are attached to larger grains. Their presence reduces the flowability of the powder and adversely affects the microstructure of the sprayed coating. The cross-section of the powder grains does not reveal any pores and inclusions (Figure 2b, d). Based on the analysis of the distribution of elements in the powder grains (Figure 3a), it can be concluded that all alloy components are evenly distributed and there is no presence of their oxides. The results of EDS point analysis of the chemical composition of the powder grains (Figure 3b) revealed that they differed from that declared by the manufacturer (Table 1). In the case of main components, i.e. Zr and Cu, the difference are small, but atomic share of Al is 11% lower and the share of Nb is 76% higher.

There is a very large variation in the size of the powder grains, which adversely affects the microstructure and properties of cold sprayed coatings. As can be seen in Figure 4, their range is 5–90 μm with parameters $d_{10} = 12.8 \text{ \mu m}$, $d_{50} = 26.9 \text{ \mu m}$ and $d_{90} = 63.2 \text{ \mu m}$. The grain size range is much larger than the manufacturer’s [25]. Such a wide

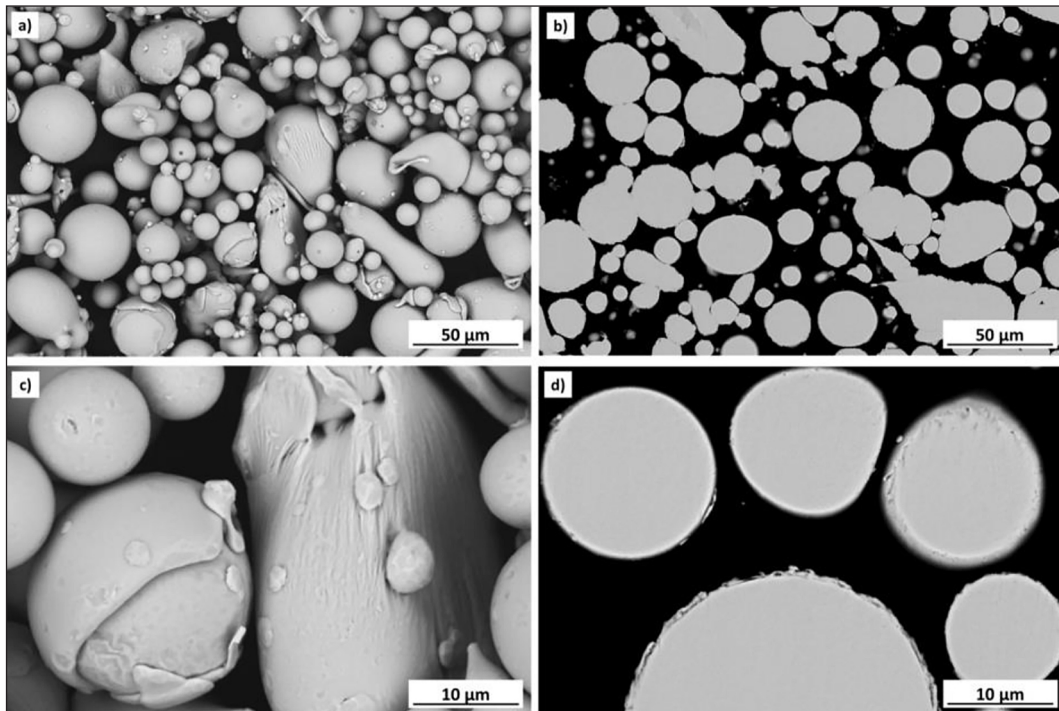


Figure 2. Microstructure of the AMZ4 powder; (a) grain morphology, (b) grain cross-section, (c) morphology of single grain, (d) cross-section of single grain

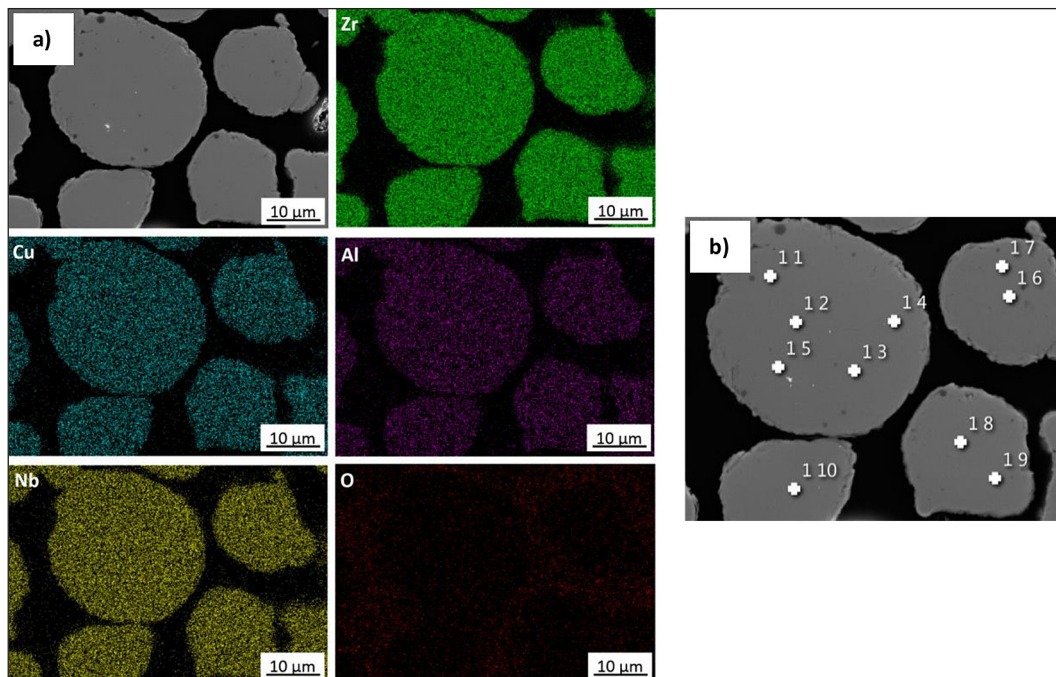


Figure 3. AMZ4 powder grains: (a) distribution of elements, (b) EDS point analysis measurement locations

range of grain sizes can be used in laser processes [26, 27, 29] but in the case of cold gas spraying it should be narrowed down to smaller sizes e.g. 15–30 μm. Figure 5 presents the X-ray diffraction pattern recorded for AMZ4 powder with halo peak which indicates its amorphous structure.

Microstructure of cold sprayed AMZ4 coating

Figure 6a presents the microstructure of the cold sprayed amorphous AMZ4 coating. The thickness of the sprayed coating was $493 \pm 34 \mu\text{m}$. There are almost invisible boundaries between

Table 1. Results of powder grains EDS point analysis, at.%

Spectrum label	Zr	Cu	Al	Nb	Total
1 1	59.64	28.56	9.44	2.35	100.00
1 3	59.11	29.25	8.97	2.68	100.00
1 2	58.92	29.13	9.17	2.77	100.00
1 4	58.32	29.71	9.33	2.64	100.00
1 5	58.64	29.39	9.33	2.64	100.00
1 8	58.91	29.04	9.35	2.70	100.00
1 7	58.37	29.53	9.36	2.75	100.00
1 6	59.13	29.07	9.25	2.55	100.00
1 9	58.74	29.30	9.18	2.79	100.00
1 10	58.42	29.89	9.12	2.58	100.00
Average value	58.82 ± 0.39	29.29 ± 0.26	9.25 ± 0.13	2.64 ± 0.12	100.00

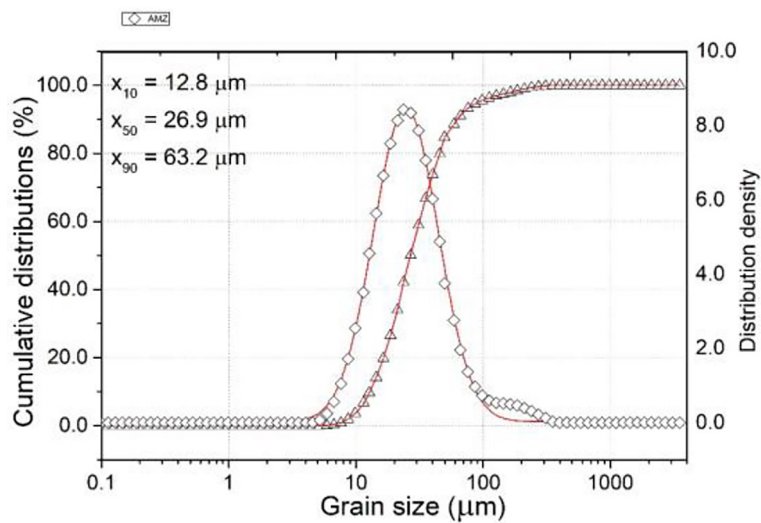


Figure 4. Particle size distribution of AMZ4 powder

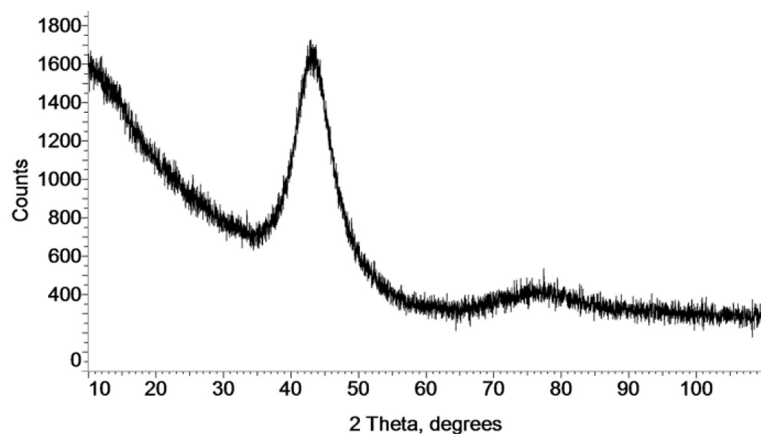


Figure 5. X-ray diffraction of AMZ4 powder

the lamellas (Fig. 6b, c). The sprayed amorphous particles formed a very dense coating, and the deformed particles strongly adhered to the substrate (Fig. 6d). The black phase visible on the interface

is the remains of alumina grains used in the grit-blasting process. The small number of pores that are visible close to the surface of the coating is the result of the lack of compaction of the coating

by subsequently impacting powder grains (Fig. 6a, b). Porosity of deposited coating was 0.8 %.

A cross-section of the AMZ4 coating after etching shows its more detailed microstructure (Figure 7). Upon impact onto the surface, most particles, even very large ones (white arrow), experienced significant plastic deformation and flattening and, as lamellae, constitute a basic element of the coating microstructure. However, there are also a few particles visible there that, despite their small size, have not been deformed and have retained a spherical or almost spherical shape (red arrows). The different lamella morphology is directly related to the velocity and temperature of

the grain when it hits the substrate. This is also influenced by the grain size, the properties and morphology of the substrate [30, 31]. Furthermore, this variation in the behaviour of the impact grains causes the formation of pores, which are an inherent element of all thermally sprayed coatings. The pores between the strongly deformed lamellae are clearly visible (yellow arrows). Depending on these factors, metallurgical bonds (white arrows) or nanogaps (red arrows) are formed between the lamellae (Fig. 7b). Although the AMZ4 coating microstructure is typical for those obtained by cold spray process, as for standard metal powders having a crystalline structure, the coating formation

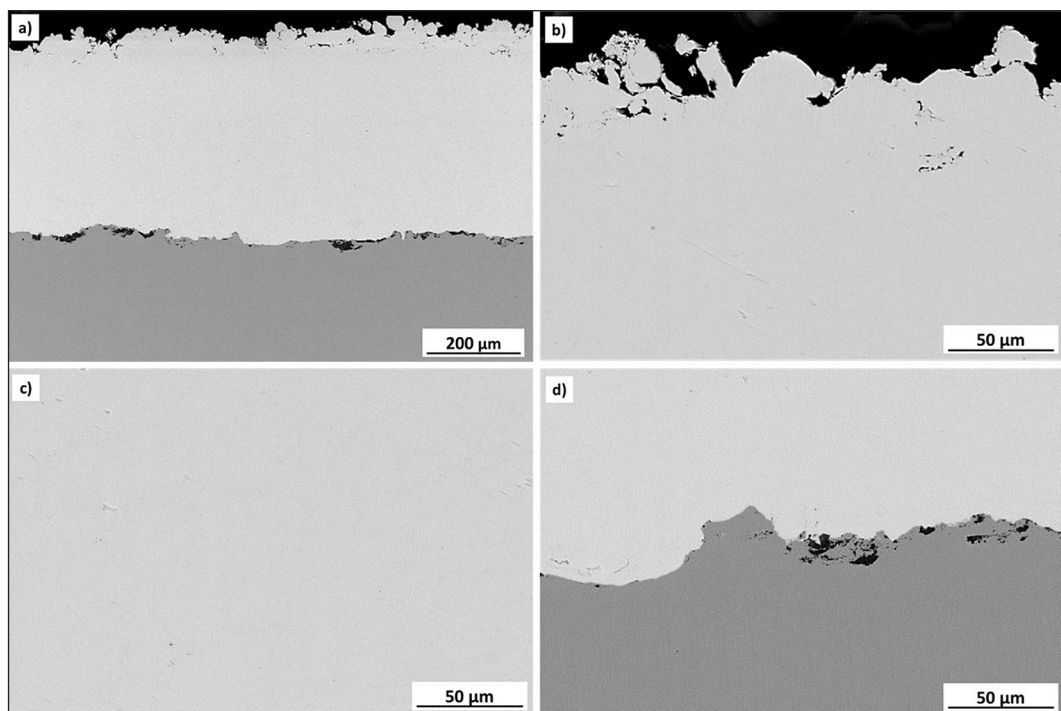


Figure 6. Cross-section of AMZ4 coating; (a) microstructure, (b) upper part, (c) middle part, (d) interface coating-substrate

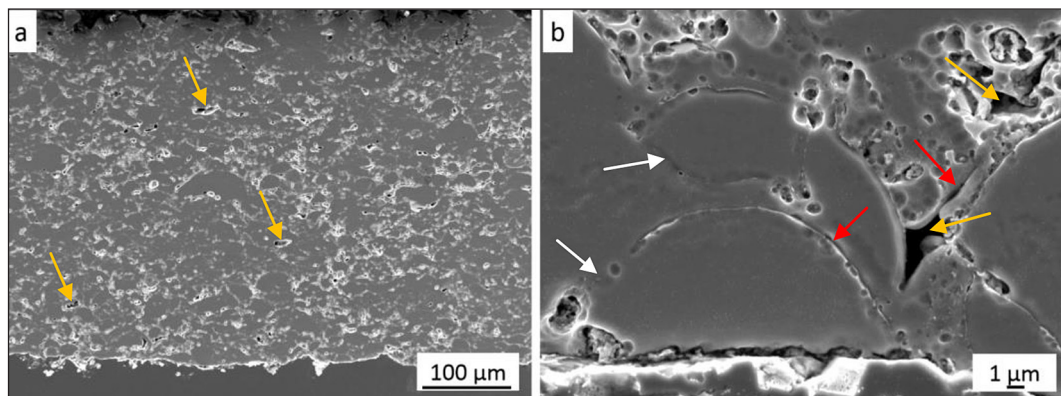


Figure 7. Cross-section of etched AMZ4 coating; (a) microstructure, (b) interface coating-substrate

mechanism in the case of amorphous feedstock is different. In the first case, bonding of particles to a substrate and then next to the deposited layer is related to the adiabatic shear instability process that occurs under the condition of extremely high plastic deformation rate when the grain hits the substrate [10, 11, 16]. However, such a coating construction mechanism cannot occur in the case of amorphous powders. In this case, the deposition behaviour of amorphous grains is governed by viscous flow and melting at the interface supported by adiabatic heat generation. The viscosity and velocity of particles at the moment of impact directly on this process. As a result, metallurgical bonding is created [1, 4, 32]. Depending on the course of this process, nanocrystallization in this area may occur [33].

Based on the analysis of the coating-substrate interface, it can be concluded that there are no metallurgical bonds between AMZ4 lamellae and 1H18N9T steel substrate. The gap is much larger than in the case of direct contact between lamellas. It can be assumed that the adhesion of the AMZ4 coating is solely the result of the anchoring of the lamellas in the roughness of the grit-blasted steel substrate (Figure 7b).

Figure 8a presents the EDS mapping of cold sprayed AMZ4 coating. The distribution of elements is uniform, and there is no segregation of them. There is also no evidence that the powder

grains were oxidized during the cold spray. This conclusion was further confirmed by EDS point analysis (Figure 8b). All elements are evenly distributed over the entire thickness of the deposited coating. Moreover, there was no change in their share to the content in the sprayed powder (Tab. 2).

The surface of cold sprayed AMZ4 coating is presented in Fig. 9. SEM examinations of the surface showed that the internal structure of the powder grains has a considerable effect on the obtained surface microstructure. The degree of plastic deformation depends on the grain size. Grains of a size not exceeding 10 μm in diameter did not acquire sufficient velocity, i.e. they did not exceed the critical velocity v_{kr} and were jammed in the unevenness of the coating surface or bounced off (Figure 9a, b, c). Traces of the remnants of the reflected grains are visible in the form of “vein patterns” (Figure 9c). Such a case of metallurgical bonding residue was also reported by Fan et al. [33] for a crater left by a single grain of amorphous Zr-based alloy on a polished aluminium substrate. Cracked lamellae are also visible (Figure 9b, d); the energy during impact was too low for a viscous fluid. Inhomogeneous deformation typical for metallic glasses occurred, causing shear cracks. Strongly deformed grains of AMZ4 powder are well seen at higher magnification with shear bands and shear cracks (Figure 9d). These thin lamellae are proof for the viscous

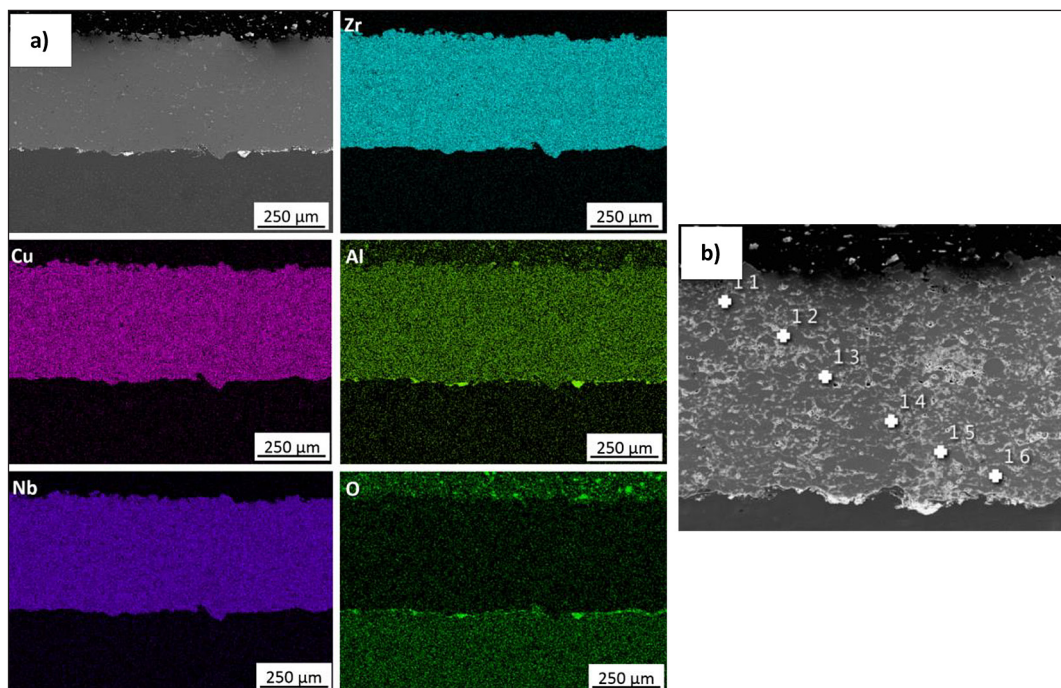


Figure 8. AMZ4 cold spray coating: (a) distribution of elements, (b) EDS point analysis measurement locations

Table 2. Results of AMZ4 cold spray coating EDS point analysis, at.%

Spectrum label	Zr	Cu	Al	Nb	Total
1 1	58.61	29.48	9.24	2.67	100.00
1 2	57.32	31.52	8.34	2.82	100.00
1 3	58.82	29.23	9.21	2.74	100.00
1 4	58.84	29.05	9.48	2.63	100.00
1 5	58.81	29.03	9.46	2.69	100.00
1 6	59.47	28.17	9.90	2.46	100.00
Average value	58.65 ± 0.65	29.41 ± 1.02	9.27 ± 0.47	2.67 ± 0.11	100.00

fluid or melting fluid and homogenous deformation of amorphous particles if energy of impact with the ground is appropriate (Fig. 9c, d) [23]. Their deformation during impact on the substrate eliminates or significantly reduces the voids in the coating and reduces its porosity. The regular shape of the grains produces well seen pores between the deformed particles indicating a negligible porosity of coatings.

Figure 10 shows the X-ray pattern of the deposited AMZ4 coating. There are no sharp peaks indicating the presence of crystalline phases similarly as in the case with sprayed AMZ4 powder (Fig. 5). This proves that in the cold spray process it is possible to completely preserve the amorphous structure of the AMZ powder grains in the coating. This is a unique advantage of cold spray process. It is usually impossible to completely

maintain the initial structure possible when using laser techniques to obtain bulk metallic glasses in additive manufacturing processes [25–27].

Surface topography of cold sprayed AMZ4 coating

Figure 11 presents surface topography, depth histogram and bearing curve for the AMZ4 cold sprayed coating. There is significant variation in the surface topography resulting from the deposition process and the varying degrees of deformation of the powder grains (Fig. 11a). The surface topography picture is consistent with Fig. 6b and Fig. 9c, where significant unevenness of amorphous coating is visible. This is the result of jamming of undeformed amorphous grains with diameters up to 10 μm on the coating surface, which

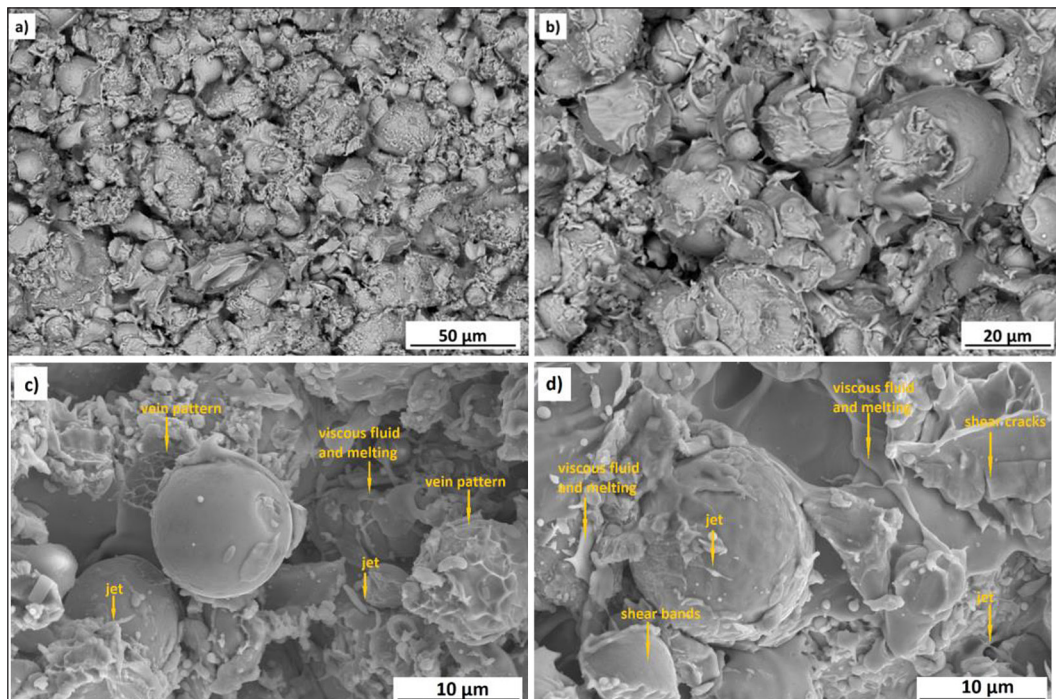


Figure 9. Morphology of surface AMZ4 coating; (a) mag. 200x, (b) mag. 500x, (c) mag. 5000x, (d) mag. 5000x

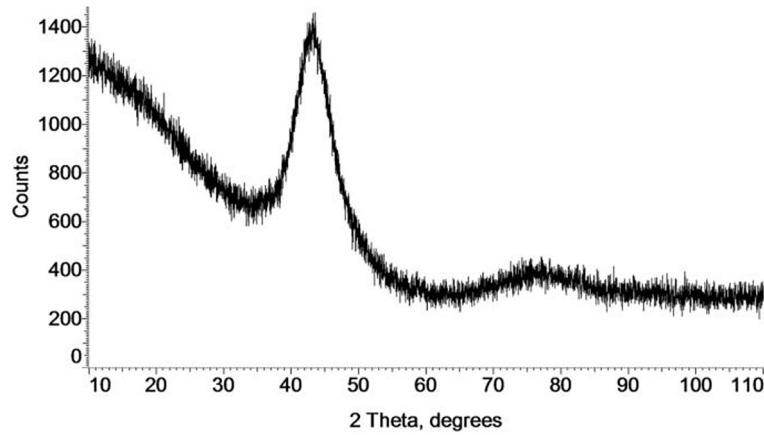


Figure 10. X-ray diffraction of AMZ4 coating

are also visible in the coating microstructure (Fig. 6a). Larger grains are significantly deformed and did not cause an increase in the unevenness of coating surface. These observations are consistent with depth histogram and bearing curve for AMZ4 coating (Figure 11b). Height parameters of surface were calculated using all the measurement data from the optically scanned surface area, according to ISO 25178 (Table 3). The arithmetic mean of the height (S_a) describing the height changes for the cold sprayed AMZ4 coatings and root mean square surface height (S_q) are in the

lower range of values for cold sprayed coatings [34–36]. The skewness parameter S_{sk} is positive, which indicates the concentration of material near the profile top and is higher than for the compared cold gas sprayed coatings (Table 3). Similarly, in the case of a much higher value of kurtosis S_{ku} which is the result of the presence of grooves in the profile of the surface, which are remnants of undeformed grains and coatings porosity. The maximum peak height S_p values are different for the analysed coatings. The other topography parameters, such as the maximum valley depth S_v

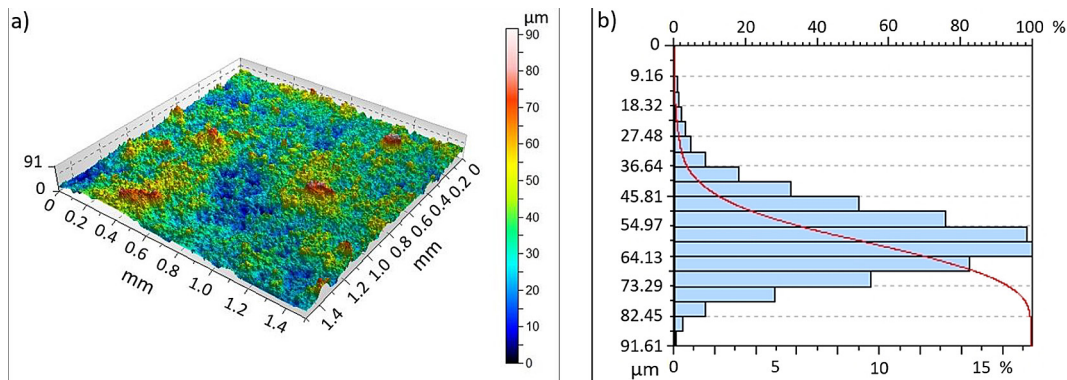


Figure 11. AMZ4 cold sprayed coating: (a) surface topography, (b) depth histogram with bearing curve

Table 3. Parameters of cold sprayed coatings surface according to ISO 25178

Coating	Height parameters						
	S_a (μm)	S_q (μm)	S_{sk}	S_{ku}	S_p (μm)	S_v (μm)	S_z (μm)
AMZ4	8.57	11.05	0.65	4.08	58.25	33.36	91.61
Ni [34]	12.3	15.3	0.08	2.74	51.5	58.5	110
Cr_3C_2 -25(Ni20Cr) [35]	10.2	12.8	-0.31	3.2	43.0	69.4	112.4
Ni20Cr [36]	10.04	12.73	-0.07	3.23	59.20	73.37	131.57

Note: S_a – arithmetic mean height, S_q – root mean squared height, S_{sk} – skewness, S_{ku} – kurtosis, S_p – maximum peak height, S_v – maximum valley depth, S_z – maximum height.

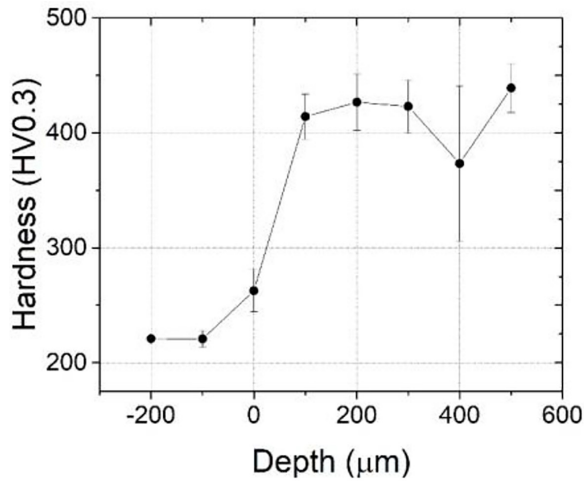


Figure 12. Hardness distribution of AMZ4 coating

and the maximum height, are lower compared to cold sprayed coatings [34–36].

Hardness of cold sprayed AMZ4 coating

The Vickers microhardness variation in the amorphous AMZ4 coating deposited by cold spraying as a function of the distance from the interface to the surface are shown in Figure 12.

An increase in Vickers microhardness is visible in the 1H18N9T steel substrate near the interface. The microhardness of the substrate is 221 HV0.3, and at the interface, it increases to 263 HV0.3. The increase in microhardness is due to two factors related to the preparation of the substrate and the spraying process. The first factor is the grit-blasting operation before spraying, which causes the work hardening at the substrate surface. The next one concerns the impact of high-speed powder grains on the substrate. This interaction of powder grains generates additional plastic deformation of the substrate and work hardening, which increases microhardness by about 20%. Near the interface the microhardness of amorphous coating is 414 HV0.3 and at its surface 439 HV0.3. There is a clear drop in microhardness to 373 HV0.3 at 100 µm from the surface, which is related to the porosity of the coating at the measurement points (significant standard deviation).

The nanoindentation and elastic modulus maps (Fig. 13a, c) with histograms (Fig. 13b, d) for AMZ4 coating are presented in Fig. 13. A square grid for nanoindentation tests on the cross-sections of the coating was applied. As a result of measurements, values of 6.25 ± 0.39 GPa and 100.18 ± 7.58

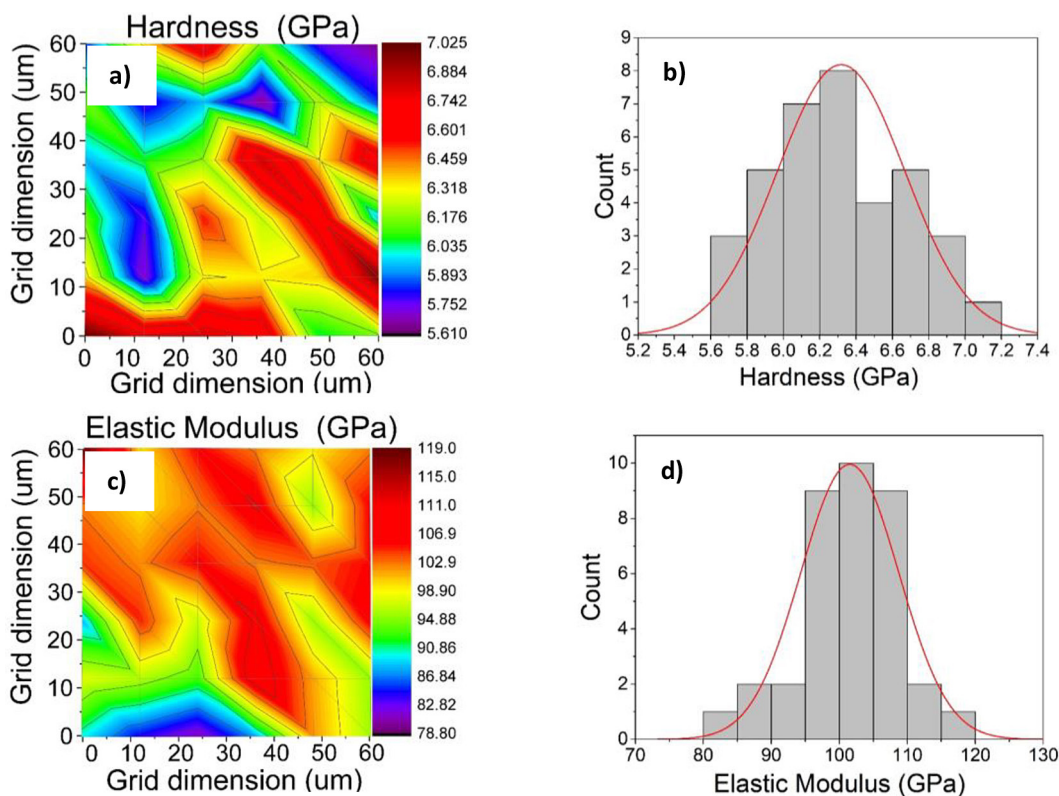


Figure 13. Distribution of the mechanical properties for AMZ4 coating; (a) hardness map, (b) hardness histogram, (c) elastic modulus map, (d) elastic modulus histogram

GPa were obtained, respectively. The level of the obtained values is comparable to that of an amorphous alloy of similar composition ($Zr_{55}Al_{10}Ni_5Cu_{30}$) obtained by the arc melting, 6.2 ± 0.1 GPa and 114.5 ± 2 GPa, respectively [37]. Based on the analysis of the maps obtained, it can be concluded that there are significant differences in both mechanical properties of cold sprayed AMZ4 coating in micro areas. Local changes of these values result from different degrees of deformation of powder grains when they hit the substrate. The coating microstructure is composed of lamellae of different thicknesses and undeformed grains that are stuck together in the coating. The form of bonding between them and the presence of pores are also important. Moreover, the shot peening effect (particles rebounding off the surface) strengthens the coating microstructure. All these factors cause significant variations in the mechanical properties of the amorphous coating during the nanoindentation test.

CONCLUSIONS

The following conclusions can be drawn based on the microstructure analysis and mechanical properties tests of cold sprayed amorphous coatings. The cold spraying process enables the deposition of amorphous coatings with a uniform distribution of elements through the volume. The use of powder without fine grain fractions should allow for obtaining a more uniform microstructure of the amorphous coating and improve its mechanical properties.

The cold sprayed coating retained the complete amorphous structure of the powder used. No new phases or oxides were detected. Most of height parameters of AMZ4 coating surface were lower compared to cold sprayed coatings but parameters Ssk and Sku revealed higher values.

The microhardness of the cold sprayed amorphous coating was almost twice as high as that of 1H18N9T steel. The nanohardness and elastic modulus of the coating are comparable to that of an amorphous alloy of similar composition ($Zr_{55}Al_{10}Ni_5Cu_{30}$) obtained by the arc melting.

Acknowledgements

The work reported herein was supported by project No. 01.1.05.00/1.02.001/SUBB.MCKE.24.003 funded by the Ministry of Education and Science, Poland.

REFERENCES

1. Xiulin J., Yiping S., Cuicui J., Hui W. Zhanxi Z. Slurry erosion behavior of two Zr-based bulk metallic glasses. *Wear*, 2021; 476: 203684. <https://doi.org/10.1016/j.wear.2021.203684>
2. Gao K., Zhu X.G., Chen L., Li W.H., Xu X., Pan B.T., Li W.R., Zhou W.H., Li L., Huang W., Li Y. Recent development in the application of bulk metallic glasses. *Journal of Materials Science & Technology* 2022; 131: 115–121. <https://doi.org/10.1016/j.jmst.2022.05.028>
3. Hejwowski T., Marczevska-Boczkowska K., Kobayashi A. A comparative study of electrochemical properties of metallic glasses and weld overlay coatings. 2013; 88: 118–123. doi: <https://doi.org/10.1016/j.vacuum.2012.02.031>
4. Sohrabi S., Fu J., Li L., Zhang Y., Li X., Sun F., Ma J., Wang W.H. Manufacturing of metallic glass components: Processes, structures and properties. *Progress in Materials Science* 2024; 144: 101283. <https://doi.org/10.1016/j.pmatsci.2024.101283>
5. Liu H., Jiang Q., Huo J., Zhang Y., Yang W., Li X. Crystallization in additive manufacturing of metallic glasses: A review. *Additive Manufacturing*, 2020; 36: 101568. <https://doi.org/10.1016/j.addma.2020.101568>
6. Lashgari, H.R., Ferry, M., Li, S. Additive manufacturing of bulk metallic glasses: Fundamental principle, current/future developments and applications. *Journal of Materials Science & Technology* 2022; 119: 131–149. <https://doi.org/10.1016/j.jmst.2021.09.068>
7. Papyrin, A. *Cold Spraying*. Elsevier Ltd. Amsterdam, The Netherlands, 2007.
8. Pawlowski, L. *The science and engineering of thermal spray coatings*. 2nd ed.; Wiley: Hoboken, NJ, USA, 2008.
9. Stoltenhoff T., Voyer M., Kreye H. Cold spraying – State of the art and applicability, *Proceedings of the International Thermal Spray Conference Essen*, 2002; 366–374.
10. Srikanth A., Bolleddu V. A review on characteristics of cold sprayed coatings. *Australian Journal of Mechanical Engineering*. <https://doi.org/10.1080/14484846.2020.1794504>
11. Vaz R.F., Garfias A., Albaladejo V., Sanchez J., Cano I.G. A review of advances in cold spray additive manufacturing. *Coatings* 2023; 13: 267. <https://doi.org/10.3390/coatings13020267>
12. Żórawski W., Molak R., Mądry J., Sienicki J., Góral A., Makrenek M., Scendo M., Dobosz R. Experimental and numerical investigations of titanium deposition for cold spray additive manufacturing as a function of standoff distance. *Materials* 2021; 14: 5492. <https://doi.org/10.3390/ma14195492>

13. Zarazua-Villalobos L., Mary N., Bernard C., Ogawa K., Boissy C. Improved deposition efficiency of low-pressure cold-sprayed tin coating through powder recycling. *Journal of Thermal Spray Technology* 2022; 31: 2577–2593. <https://doi.org/10.1007/s11666-022-01447-4>
14. Li W., Yang K., Yin S., Yang X., Yaxin Xu Y., Lupoi R. Solid-state additive manufacturing and repairing by cold spraying: A review. *Journal of Materials Science & Technology* 2018; 34(3): 440–457. <https://doi.org/10.1016/j.jmst.2017.09.015>
15. Prashar G., Vasudev H. A comprehensive review on sustainable cold spray additive manufacturing: State of the art, challenges and future challenges. *Journal of Cleaner Production* 2021; 310: 127606. <https://doi.org/10.1016/j.jclepro.2021.127606>
16. Guo D., Kazasidis M., Hawkins A., Fan N., Leclerc Z.Z., MacDonald D., Nastic A., Nikbakht R., Ortiz-Fernandez R., Rahmati S., Razavipour M., Richer P., Yin S., Lupoi R., Jodoin B. Cold spray: over 30 years of development toward a hot future. *Journal of Thermal Spray Technology*. <https://doi.org/10.1007/s11666-022-01366-4>
17. Sienicki J., Żórawski W., Dworak A., Koruba P., Jurawicz P., Reiner J. Cold spraying and laser cladding in the aircraft coating production as an alternative to harmful cadmium and chromium electroplating processes. *Aircraft Engineering and Aerospace Technology*, 2019; 91: 205–215.
18. Bijalwan P., Kumar A., Nayak S.K., Banerjee A., Dutta M., Laha T. Microstructure and corrosion behavior of Fe-based amorphous composite coatings developed by atmospheric plasma spraying. *Journal of Alloys and Compounds* 2019; 796: 47–54. <https://doi.org/10.1016/j.jallcom.2019.05.046>
19. Su J., Kang J., Yue W., Ma G., Fu Z., Zhu L., She D., Wang H., Wang C. Comparison of tribological behavior of Fe-based metallic glass coatings fabricated by cold spraying and high velocity air fuel spraying. *Journal of Non-Crystalline Solids* 2019; 522: 119582. <https://doi.org/10.1016/j.jnoncrysol.2019.119582>
20. Wang Z., Ma L., Han B., Huang G., Cao Q., Sun M. Influence of parameters on the cold spraying FeCoCrMoBCY amorphous coatings. *Surface Engineering* 2021; 37(5): 545–557. <https://doi.org/10.1080/02670844.2020.1805716>
21. Babu P.S., Jha R., Guzman M., Sundararajan G., Agarwal A. Indentation creep behavior of cold sprayed aluminum amorphous/ nano-crystalline coatings. *Materials Science & Engineering A* 2016; 658: 415–421. <http://dx.doi.org/10.1016/j.msea.2016.02.030>
22. Yoon S., Lee C., Choi H., Jo H. Kinetic spraying deposition behavior of bulk amorphous NiTiZrSiSn feedstock. *Materials Science & Engineering A* 2006; 415: 45–52.
23. List, A., Gärtner, F., Mori, T., Schulze, M., Assadi, H., Kuroda, S., Klassen, T. Cold spraying of amorphous Cu50Zr50 alloys. *Journal of Thermal Spray Technology* 2014; 24: 108–118. <https://doi.org/10.1007/s11666-014-0187-x>
24. Marattukalam, J.J., Pacheco V., Karlsson D., Riekehr L., Lindwall J., Forsberg F., Jansson F., Sahlberg M., Hjärvarsson B. Development of process parameters for selective laser melting of a Zr-based bulk metallic glass. *Additive Manufacturing* 2020; 33: 101124. <https://doi.org/10.1016/j.addma.2020.101124>
25. Sohrabi N., Jhabvala J., Kurtuldu G., Stoica M., Parrilli A., Berns S., Polatidis E., Van Petegem S., Hugon S., Neels A., Loffer J.F., Loge R. Characterization, mechanical properties and dimensional accuracy of a Zr-based bulk metallic glass manufactured via laser powder-bed fusion. *Materials and Design* 2021; 199: 109400. <https://doi.org/10.1016/j.matdes.2020.109400>
27. Luo D., Du Y. Mechanical properties of bulk metallic glasses additively manufactured by laser powder bed fusion: A review. *Materials* 2023; 16: 7034. <https://doi.org/10.3390/ma16217034>
28. Best J.P., Nomoto K., Yang F., Li B., Stolpe M., Zeng L., Evenson Z., Hugenschmidt C., Li X., Ronger S.P., Kruzic J.J. Advanced structural analysis of a laser additive manufactured Zr-based bulk metallic glass along the build height. *Journal of Materials Science* 2022; 57: 9678–9692. <https://doi.org/10.1007/s10853-022-06991-6>
29. Pacheco V., Karlsson D., Marattukalam J.J., Stolpe M., Hjärvarsson B., Jansson Ulf., Sahlberg M. Thermal stability and crystallization of a Zr-based metallic glass produced by suction casting and selective laser melting. *Journal of Alloys and Compounds* 5 June 2020; 825: 153995. <https://doi.org/10.1016/j.jallcom.2020.153995>
30. Heraeus Additive Manufacturing GmbH, www.heraeus-amloy.com, Met. Powder AMZ4 Data Sheet. 2023.
31. Żórawski W., Góral A., Makrenek M., Lityńska-Dobrzyńska L., Czaja P., Influence of preheating gas temperature and surface roughness on microstructure and mechanical properties of cold sprayed nickel coatings. *Materials* 2023; 16: 7002.
32. Scendo M., Żórawski W., Staszewska K., Makrenek M., Góral A. Influence of Surface Pretreatment on the Corrosion Resistance of Cold Sprayed Nickel Coatings in Acid Chloride Solution. *J. Mater. Eng. Perf.* 2018; 27: 1725–1737.
33. Su J., Kang J., Yue W., Ma G., Fu Z., Zhu L., She D., Wang H., Wang C. Review of cold spraying and its use for metallic glass coatings. *Materials Science and Technology* 2019; 35(16): 1908–1923. <https://doi.org/10.1080/02670836.2019.1654240>
34. Fan N., Huang C., Wang Z., Yu P., Chen W., Luppoi

- R., Xie Q., Liu L., Yin S. Interparticle bonding and interfacial nanocrystallization mechanisms in additively manufactured bulk metallic glass fabricated by cold spray. *Additive Manufacturing* 2022; 58: 103057. <https://doi.org/10.1016/j.addma.2022.103057>
35. Góral A., Żórawski W., Czaja P., Lityńska-Dobrzyńska L., Makrenek M., Kowalski S. Effect of powder morphology on the microstructure and properties of cold sprayed Ni coatings. *International Journal of Materials Research*, 2019; 1101: 49–59, <https://doi.org/10.3139/146.111698>
36. Góral A., Żórawski W., Makrenek M. The effect of the standoff distance on the microstructure and mechanical properties of cold sprayed Cr₃C₂-25(Ni20Cr) coatings. *Surface and Coatings Technology* 2019; 361: 9–18.
37. Soboń D. Effect of laser surface melting on microstructure of cold sprayed Ni20Cr coatings. *Archives of Metallurgy and Materials* 2021; 66: 853–860.
38. Ji X., Shan Y., Ji C., Wang H., Zhao Z. Slurry erosion behavior of two Zr-based bulk metallic glasses. *Wear* 2021; 476: 203684. <https://doi.org/10.1016/j.wear.2021.203684>